Effective Mass Anisotropy of Hot Electrons in Nonparabolic Conduction Bands of *n*-Doped InGaAs Films Using Ultrafast Terahertz Pump-Probe Techniques

F. Blanchard,[1,*] D. Golde,[2] F. H. Su,[3,†] L. Razzari,[1,‡] G. Sharma,[1] R. Morandotti,[1] T. Ozaki,[1] M. Reid,[4] M. Kira,[2] S. W. Koch,[2] and F. A. Hegmann[3,§]

[1]*INRS-EMT, Advanced Laser Light Source, Université du Québec, Varennes, Québec J3X 1S2, Canada*
[2]*Department of Physics, Philipps-University, Renthof 5, 35032 Marburg, Germany*
[3]*Department of Physics, University of Alberta, Edmonton, Alberta T6G 2G7, Canada*
[4]*Department of Physics, UNBC, Prince George, British Columbia V2N 4Z9, Canada*

(Received 29 October 2010; revised manuscript received 20 April 2011; published 31 August 2011)

The anisotropic effective mass of energetic electrons in an isotropic, nonparabolic conduction band is revealed using ultrafast THz-pump–THz-probe techniques in a *n*-doped InGaAs semiconductor thin film. A microscopic theory is applied to identify the origin of the observed anisotropy and to show that the self-consistent light-matter coupling contributes significantly to the THz response.

DOI: 10.1103/PhysRevLett.107.107401 PACS numbers: 78.47.jh, 73.50.Fq, 78.40.Fy, 78.47.N−

Terahertz (THz) field-induced transport effects can strongly influence the behavior of fast semiconductor components operating under extreme conditions [1,2]. High-field transport dynamics of the charge carriers in such devices is, among other things, determined by the band structure of the solid. Consequently, a complete understanding of the underlying physical processes requires a detailed knowledge of the band structure. In recent years, the development of extremely strong pulsed THz sources and ultrafast coherent detection methods [3,4] has made it possible to continuously alter the electron momentum across the Brillouin zone. Using various techniques of time-resolved THz nonlinear spectroscopy [3–20], effects such as extreme THz nonlinearities [5–9], THz-pulse-induced intervalley scattering [12–15], and ballistic transport of electrons across half of the Brillouin zone [16] have been investigated in semiconductors. Some of these effects can be accessed by using optical-pump–THz-probe (OPTP) [13,21–24] as well as THz-pump–optical-probe setups [8–10]. Currently, THz-pump–THz-probe (TPTP) techniques seem very attractive in probing nonlinear carrier dynamics induced by intense few-cycle THz pulses in semiconductors, such as impact ionization in InSb [19] as well as intervalley scattering in doped GaAs, Si, and Ge [14].

The high-field electron transport is very much defined by the diagonal part of the inverse effective-mass tensor $m_i^{-1}(\mathbf{k}) \equiv m_{i,i}^{-1}(\mathbf{k}) = \frac{1}{\hbar^2}\frac{\partial^2 \varepsilon_{\mathbf{k}}}{\partial k_i^2}$ [25] where $\varepsilon_{\mathbf{k}}$ is the electron energy and $\mathbf{k}$ is the electron wave vector. More than 50 years ago, magnetic cyclotron resonance (CR) revealed that the Brillouin zone boundaries of Si and Ge produce conduction bands with ellipsoidal constant energy surfaces and therefore highly anisotropic $m_i(\mathbf{k})$ [26,27]. For most III–V semiconductors, however, the conduction band $\varepsilon_{\mathbf{k}}$ at the Γ point is considered to be isotropic (i.e., spherically symmetric such that $\varepsilon_{\mathbf{k}} = \varepsilon_{|\mathbf{k}|}$) but nonparabolic [25]. Even though CR has also been used to determine band nonparabolicity factors in these materials [28–30], CR probes the average effective mass (often called cyclotron mass) for a given orbit in k space and for a certain level of energy. Therefore, it cannot probe the anisotropy of electron effective mass $[m_x(\mathbf{k}) \neq m_y(\mathbf{k})]$ caused by nonparabolicity in bands with spherical constant energy surfaces.

Figure 1 illustrates the origin of this mass anisotropy in an isotropic but nonparabolic conduction band for electron motion in the k_x-k_y plane [Fig. 1(a)]. If an electron is accelerated in the x direction to $\mathbf{k}_0 = k_0\hat{\mathbf{x}}$, the masses $m_x(\mathbf{k}_0)$ and $m_y(\mathbf{k}_0)$ become different for any nonparabolic band simply because the curvatures of the band along k_x [plane A, Fig. 1(b)] and k_y [plane B, Fig. 1(c)] are different at the point $\mathbf{k}_0$. This results in an effective-mass anisotropy, $m_x(\mathbf{k}_0) > m_y(\mathbf{k}_0)$, for highly excited electrons as shown in Fig. 1(d). Since the mass anisotropy only appears away from the Γ point and increases with k_0 [Fig. 1(d)], one typically needs strong electric fields driving the electrons to sufficiently high k_0 in order to observe this effect. Note that the effective-mass anisotropy disappears completely at all $\mathbf{k}$ if the band is parabolic.

In this Letter, we present a new technique that enables us to reveal the effective-mass anisotropy of energetic electrons in an isotropic, nonparabolic conduction band. We implement a polarization-dependent TPTP experiment as shown schematically in Fig. 1(e). Here, a strong THz-pump pulse accelerates the electrons in the x direction which are then probed by another weaker THz pulse polarized either in the x (colinear, CL) or y (cross-linear, XL) direction. We show that the anisotropy of the electron effective masses induced by the THz-pump pulse yields distinctly different THz-probe responses for the CL and XL configurations because the measured THz-probe signal is proportional to the corresponding component of $m_i^{-1}(\mathbf{k})$. While the nonlinear THz response in doped semiconductors arising from band nonparabolicities has already been reported [31,32],

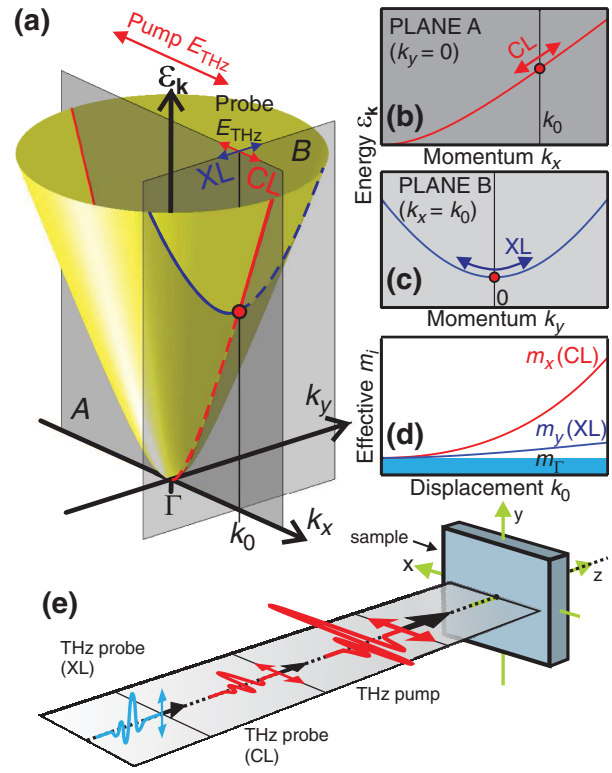

FIG. 1 (color). (a) Schematic of an isotropic, nonparabolic conduction band with an electron excited in the k_x-k_y plane to $\mathbf{k}_0 = k_0\hat{\mathbf{x}}$. (b) Schematic dispersion relation for the electron along k_x within plane A and (c) along k_y within plane B. (d) The corresponding effective masses m_x and m_y together with the Γ-point mass m_Γ (shaded area). (e) Polarization-dependent TPTP configuration. The large electric field of the THz-pump pulse drives electrons high in the band along the x axis. The polarization of the THz-probe pulse can then be set to monitor carrier motion either parallel (colinear, CL) or perpendicular (cross-linear, XL) to the THz-pump pulse polarization.

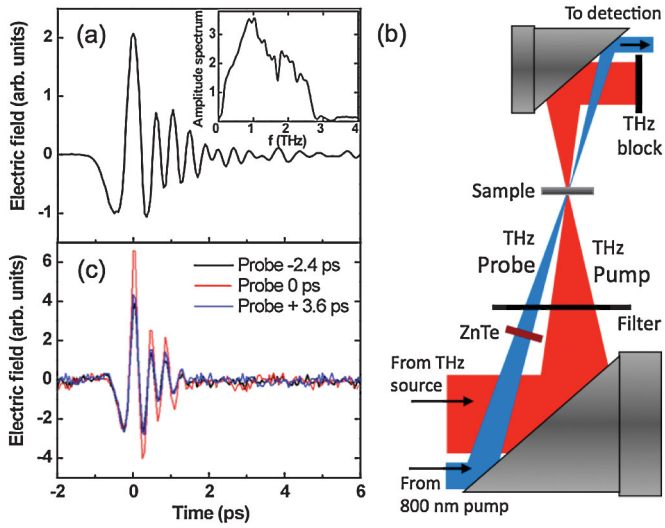

FIG. 2 (color). (a) Electric field profile of the THz-pump beam emitted by the ZnTe optical rectification source. Inset: amplitude spectrum of the THz pulse. (b) Schematic of the experimental setup. (c) Electric field profile of the transmitted THz-probe beam at various delay times between the main positive peaks of the THz-pump and THz-probe pulses.

our experimental results demonstrate the fundamental anisotropic nature of band nonparabolicity.

In our experiments, a large aperture ZnTe optical rectification source was used to generate high-power THz-pump pulses [4]. Figure 2(a) shows an example of the temporal profile of the THz pulses produced by the ZnTe source, and the inset shows the corresponding amplitude spectrum. The TPTP setup is shown schematically in Fig. 2(b). The sample used here was a 500 nm-thick n-type $In_{0.53}Ga_{0.47}As$ epilayer (carrier concentration of approximately 2×10^{18} cm^{-3}, Si dopant) on a 0.5-mm-thick [100] semi-insulating InP substrate. A $10 \times 10 \times 0.5$ mm^3 [110] ZnTe crystal placed just after the first off-axis parabolic mirror and just before the sample was used to generate a THz-probe beam that overlaps the THz-pump beam at the focus on the sample. An additional [110] ZnTe crystal 0.5 mm thick was used to detect the THz-probe pulses transmitted through the sample by free-space electro-optic sampling. The spot-size diameters on the sample for the THz-pump beam and THz-probe beam were 1.6 and 2.5 mm, respectively. Both the ZnTe source crystal and the ZnTe detection crystal for the THz-probe beam could be rotated to produce (and detect) probe polarization states either parallel or perpendicular to the THz-pump beam. At the sample position, the THz-pump and THz-probe peak electric fields were estimated to be about 200 and 2 kV/cm, respectively. The THz probe itself is in the low-field regime and therefore does not induce any nonlinear response in the sample [12,13]. We note that the noncollinear geometry of the TPTP experiment allowed the THz pump and probe beams transmitted through the sample to be spatially separated. Crosstalk between the two THz beams was therefore avoided by simply placing a metallic beam block in the path of the transmitted THz-pump beam after the second off-axis parabolic. In addition, lock-in detection of the transmitted THz-probe pulse amplitude was synchronized to an optical chopper inserted in the THz-probe source beam. As shown in Fig. 2(c), the amplitude of the transmitted THz-probe waveform increases when it overlaps with the THz-pump pulse at zero relative time delay, while the phase is relatively unaffected. This allows the transmission of the main positive peak of the THz-probe pulse to be monitored as a function of pump-probe delay time. We also note that all the experiments were performed under a dry-nitrogen purge at room temperature.

Figure 3(a) shows the normalized transmission of the main peak of the THz-probe pulse as a function of pump-probe delay time in analogy to OPTP experiments [21–24]. The presence of the THz-pump pulse results in an increase in transmission of the peak electric field of the THz-probe

pulse. The blue shaded area in Fig. 3(a) shows the transmission change for XL polarizations of pump and probe beams, while the red line shows the same measurement performed for the CL polarizations. The CL case yields a much larger amplitude oscillation than the XL case (blue area) indicating that the TPTP method can indeed access the mass anisotropy.

As previously mentioned, we have excluded the possibility that these fast oscillations are due to crosstalk between the pump and the probe at the detection level. In particular, when the probe beam is blocked, no residual signal from the pump beam is detected; both beams have to be present inside the sample in order to observe the changes in transmission. Moreover, the nonlinear signal disappears if we perform the experiment on a bare InP substrate [12].

We next apply a microscopic theory to rigorously reveal the microscopic origin of the detected anisotropy. The propagation of a THz field $\mathbf{E}(z, t)$ through a thin sample follows from the wave equation

$$\left[\frac{\partial^2}{\partial z^2} - \frac{n_b^2}{c^2}\frac{\partial^2}{\partial t^2}\right]\mathbf{E}(z, t) = \mu_0 \delta(z)\frac{\partial}{\partial t}\mathbf{J}(t), \qquad (1)$$

with the background refractive index n_b, the speed of light c, the vacuum permeability μ_0, and the excited current density $\mathbf{J}(t)$. The temporal evolution of $\mathbf{J}$ follows from $\mathbf{J}(t) = -\frac{|e|}{\hbar \mathcal{V}}\sum_{\mathbf{k}}(\nabla_{\mathbf{k}}\varepsilon_{\mathbf{k}})f_{\mathbf{k}}$ where $f_{\mathbf{k}}$ defines the microscopic electron distribution and $\mathcal{V}$ is the quantization volume of the semiconductor. For not too large k values, the conduction band energy dispersion is well described by $\varepsilon_{\mathbf{k}}(1 + \alpha\varepsilon_{\mathbf{k}}) = \frac{\hbar^2\mathbf{k}^2}{2m_\Gamma}$ [25] with the Γ-point effective mass $m_\Gamma = 0.04m_0$ and the nonparabolicity parameter $\alpha = 1.33\ \mathrm{eV}^{-1}$ [33] yielding significant nonparabolicity and, hence, an anisotropic m_i for elevated $\mathbf{k}$.

We compute the dynamics of the electron distribution using an equation-of-motion approach [34,35] and obtain

$$\hbar\frac{\partial}{\partial t}f_{\mathbf{k}} = |e|\mathbf{E}(0, t)\cdot\nabla_{\mathbf{k}}f_{\mathbf{k}} + \hbar\frac{\partial}{\partial t}f_{\mathbf{k}}|_{\mathrm{scatt}}. \qquad (2)$$

The first term on the right-hand side of Eq. (2) yields the acceleration of the electrons due to the THz field. This produces a time-dependent displacement of the electronic distribution in k space according to $f_{\mathbf{k}}(t) = f_{\tilde{\mathbf{k}}(t)}$ with $\frac{d}{dt}\tilde{\mathbf{k}}(t) = -\frac{|e|}{\hbar}\mathbf{E}$. From our calculations, we find a maximum displacement of about $0.11\frac{\pi}{a}$ (a being the lattice constant) which is small enough to justify the use of our band structure model. The second term of Eq. (2) includes Coulomb and phonon scattering of the accelerated electrons. This term leads effectively to a relaxation of the carriers and, thus, to a damping of the current density. As we will discuss below, however, the experimental results are almost not affected by these relaxation processes and we can omit the corresponding term in Eq. (2).

Equation (1) shows that the THz field itself entering Eq. (2) for $f_{\mathbf{k}}$ depends on the electron dynamics via the current density. Consequently, Eqs. (1) and (2) must be solved self-consistently in order to account for the back coupling of the induced fields to the carrier dynamics. Physically, this back coupling leads to a strong reflection of the THz field from the sample and concomitantly to a radiative damping [35] of the induced current density. We find effective radiative relaxation times shorter than 40 fs, implying a dominance of the radiative decay. Consequently, the results are only weakly affected by other relaxation mechanisms.

We compute the transmission of a weak THz-probe pulse in the presence of a strong pump field by numerically solving Eqs. (1) and (2) for both CL and XL TPTP configurations. We start from a Fermi-Dirac distribution for $f_{\mathbf{k}}$ at 300 K and an electron density of $2 \times 10^{18}\ \mathrm{cm}^{-3}$. Similar to the experiment, we record the peak transmission of the probe pulse for various pump-probe delay times. The results are presented in Fig. 3(b) and are in good agreement with the measured data [Fig. 3(a)] indicating that experimental deviations from an ideal collinear pump-probe geometry are small.

We find that $\mathbf{J}(t)$ produces a high reflection of the THz-probe pulse with only about 3.5% transmission in the absence of the pump pulse. At the same time, the magnitude of the current induced by the probe pulse is proportional to the inverse effective mass $m_i^{-1}(\mathbf{k})$. Therefore, the acceleration of the electrons into the nonparabolic regions

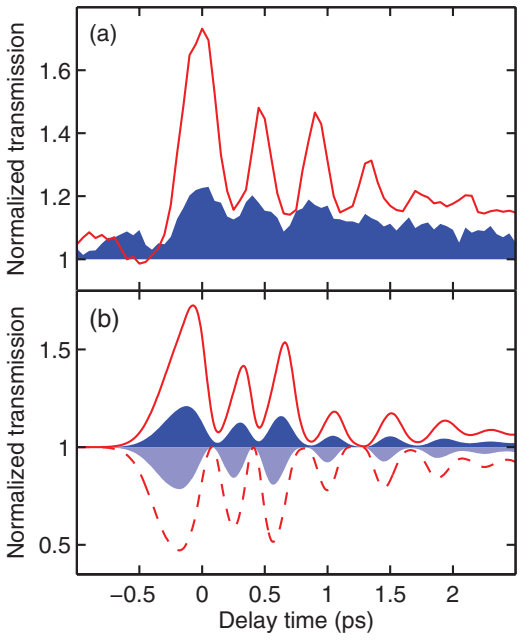

FIG. 3 (color). Measured (a) and calculated (b) normalized peak transmission of the THz-probe pulse as a function of the pump-probe delay time. The solid red lines and the blue shaded areas show the results for CL and XL TPTP configurations, respectively. The dashed red line and the light-blue shaded area in (b) represent corresponding calculations omitting radiative back-coupling effects.

can significantly modify $\mathbf{J}(t)$ and, thus, also the probe transmission detected. In particular, the solid line in Fig. 3(b) shows that the transmission is strongly enhanced for CL polarization due to the increased effective mass. The XL case (blue shaded area) produces a much smaller modification of the transmission since the effective mass is changed only moderately [see Fig. 1(d)].

In both cases, the fast oscillations directly reflect the transient pump-induced changes of the effective mass of the electrons. The theory analysis unambiguously assigns the difference of CL and XL excitations to the mass anisotropy. The slow decay—only detected in the experimental signals—results from intervalley scattering [12,13] which is not included in our model because it does not affect the detected anisotropy.

The importance of the radiative back coupling can be highlighted with an artificial calculation where we neglected these effects. Here, we simply replaced the full THz field in Eq. (2) by the external incident field. The corresponding results are shown in Fig. 3(b) as the red dashed line (CL) and the light-blue shaded area (XL). Evidently, such a simplification produces completely opposite behavior than observed in the experiment. Although the basic findings of the experiment can easily be understood intuitively by the change of the effective masses, a complete understanding requires the inclusion of the complex self-consistent back-coupling effects.

In conclusion, we have used polarization-dependent THz-pump–THz-probe techniques to study the nonlinear THz response of electrons in n-doped InGaAs. As is unambiguously confirmed by our microscopic theory, the subpicosecond time resolution of our technique, coupled with the control of probe polarization, reveals the anisotropy in effective mass of hot electrons caused by the nonparabolicity of the conduction band. This new tool may open the way to directly mapping energy bands in semiconductors. Moreover, we have shown that the inclusion of back-coupling effects is crucial to understanding the results.

We wish to acknowledge financial support from NSERC Strategic Projects, and F. B. wishes to acknowledge FQRNT (#138131). We would like to acknowledge N. Naka for helpful discussions. We are also thankful to A. Laramé and F. Poitras for their technical assistance with the ALLS laser source.

*Present address: iCeMS, Kyoto University, Yoshida-Honmachi, Sakyo-ku 606-8501 Japan.

†Present address: Institute of Solid State Physics, CAS, Hefei, Anhui, 230031, China.

‡Present address: Italian Institute of Technology, Via Morego 30, Genova 16163, Italy.

§hegmann@ualberta.ca

[1] S. D. Ganichev and W. Prettl, *Intense Terahertz Excitation of Semiconductors* (Oxford University Press, Oxford, 2006).
[2] G. L. Carr *et al.*, Nature (London) **420**, 153 (2002).
[3] M. C. Hoffmann and J. A. Fülöp, J. Phys. D **44**, 083001 (2011).
[4] F. Blanchard *et al.*, IEEE J. Sel. Top. Quantum Electron. **17**, 5 (2011).
[5] Y. Shen *et al.*, Phys. Rev. Lett. **99**, 043901 (2007).
[6] J. R. Danielson *et al.*, Phys. Rev. Lett. **99**, 237401 (2007).
[7] S. Leinß *et al.*, Phys. Rev. Lett. **101**, 246401 (2008).
[8] H. Hirori, M. Nagai, and K. Tanaka, Phys. Rev. B **81**, 081305 (2010).
[9] T. Ogawa *et al.*, Appl. Phys. Lett. **97**, 041111 (2010).
[10] A. R. Wright *et al.*, Appl. Phys. Lett. **95**, 072101 (2009).
[11] H. Wen, M. Wiczer, and A. M. Lindenberg, Phys. Rev. B **78**, 125203 (2008).
[12] L. Razzari *et al.*, Phys. Rev. B **79**, 193204 (2009).
[13] F. H. Su *et al.*, Opt. Express **17**, 9620 (2009).
[14] J. Hebling *et al.*, Phys. Rev. B **81**, 035201 (2010).
[15] M. C. Hoffmann and D. Turchinovich, Appl. Phys. Lett. **96**, 151110 (2010).
[16] W. Kuehn *et al.*, Phys. Rev. Lett. **104**, 146602 (2010).
[17] W. Feng and J. C. Cao, J. Appl. Phys. **106**, 033708 (2009).
[18] J. Liu, G. Kaur, and X.-C. Zhang, Appl. Phys. Lett. **97**, 111103 (2010).
[19] M. C. Hoffmann *et al.*, Phys. Rev. B **79**, 161201 (2009).
[20] T. Kampfrath *et al.*, Nat. Photon. **5**, 31 (2011).
[21] H. Němec *et al.*, J. Chem. Phys. **122**, 104503 (2005).
[22] S. E. Ralph *et al.*, Phys. Rev. B **54**, 5568 (1996).
[23] D. G. Cooke *et al.*, Appl. Phys. Lett. **85**, 3839 (2004).
[24] J. C. Delagnes *et al.*, J. Phys. D **42**, 195103 (2009).
[25] M. Lundstrom, *Fundamentals of Carrier Transport* (Cambridge University Press, Cambridge, 2000).
[26] G. Dresselhaus, A. F. Kip, and C. Kittel, Phys. Rev. **98**, 368 (1955).
[27] C. Hamaguchi, *Basic Semiconductor Physics* (Springer, Berlin, Heidelberg, 2010).
[28] E. D. Palik *et al.*, Phys. Rev. **122**, 475 (1961).
[29] R. J. Nicholas *et al.*, J. Phys. C **18**, L427 (1985).
[30] C. K. Sarkar *et al.*, J. Phys. C **18**, 2667 (1985).
[31] A. Mayer and F. Keilmann, Phys. Rev. B **33**, 6962 (1986).
[32] A. G. Markelz and E. G. Gwinn, J. Appl. Phys. **80**, 2533 (1996).
[33] S. Ahmed, B. Nag, and M. Roy, Solid State Electron. **28**, 1193 (1985).
[34] H. Haug and S. W. Koch, *Quantum Theory of the Optical and Electronic Properties of Semiconductors* (World Scientific, Singapore, 2009), 5th ed.
[35] M. Kira and S. W. Koch, Prog. Quantum Electron. **30**, 155 (2006).